Atmos. Meas. Tech. Discuss., 2, 439–487, 2009
www.atmos-meas-tech-discuss.net/2/439/2009/

Atmospheric Measurement Techniques Discussions

Atmospheric Measurement Techniques Discussions is the access reviewed discussion forum of *Atmospheric Measurement Techniques*

MIPAS reduced spectral resolution UTLS-1 mode measurements of temperature, O_3, HNO_3, N_2O, H_2O and relative humidity over ice: retrievals and comparison to MLS

S. Chauhan[1], M. Höpfner[1], G. P. Stiller[1], T. von Clarmann[1], B. Funke[2], N. Glatthor[1], U. Grabowski[1], A. Linden[1], S. Kellmann[1], M. Milz[1,*], T. Steck[1,], H. Fischer[1], L. Froidevaux[3], A. Lambert[3], M. L. Santee[3], M. Schwartz[3], W. G. Read[3], and N. J. Livesey[3]**

[1]Institut für Meteorologie und Klimaforschung, Forschungszentrum Karlsruhe, Germany
[2]Instituto de Astrofísica de Andalucía CSIC, Granada, Spain
[3]Jet Propulsion Laboratory, California Institute of Technology, Pasadena, California, USA

* now at: Luleå Tekniska Universitet Institutionen för Rymdvetenskap, Kiruna, Sweden
** now at: Gymnasium, Neckartenzlingen, Germany

Received: 22 December 2008 – 11 February 2009 – Published: 25 February 2009

Correspondence to: S. Chauhan (swarup.chauhan@imk.fzk.de)

Published by Copernicus Publications on behalf of the European Geosciences Union.

Abstract

During several periods since 2005 the Michelson Interferometer for Passive Atmospheric Sounding (MIPAS) on Envisat has performed observations dedicated to the region of the upper troposphere/lower stratosphere (UTLS). For the duration of November/December 2005 global distributions of temperature and several trace gases from MIPAS UTLS-1 mode measurements have been retrieved using the IMK/IAA (Institut für Meteorologie und Klimaforschung/Instituto de Astrofísica de Andalucía) scientific processor. In the UTLS region a vertical resolution of 2.5 to 3 km has been achieved. The retrieved temperature, H_2O, O_3, HNO_3, N_2O, and relative humidity over ice are intercompared with the Microwave Limb Sounder (MLS/Aura) v2.2 data. In general, MIPAS and MLS temperatures agree within ±4 K over the whole pressure range of 316–0.68 hPa. Systematic, latitude-independent differences of −2 to −4 K (MIPAS-MLS) at 121 hPa are explained by previously observed biases in the MLS v2.2 temperature retrievals. Temperature differences of −4 K up to 12 K above 10.0 hPa are present similarly in MIPAS and MLS with respect to ECMWF (European Centre for Medium-Range Weather Forecasts) and are likely due to deficiencies of the ECMWF analysis data. MIPAS and MLS stratospheric volume mixing ratios (vmr) of H_2O agree within ±1 ppmv, with indication of oscillations between 146 and 26 hPa in the MLS dataset. Tropical upper tropospheric values of relative humidity over ice measured by the two instruments differ by ±20% in the pressure range ∼146 to 68 hPa. These differences are mainly caused by the MLS temperature biases. Ozone mixing ratios agree within 0.5 ppmv (10 to 20%) between 68 and 14 hPa. At pressures smaller than 10 hPa, MIPAS O_3 vmr are higher than MLS by an average of 0.5 ppmv (10%). General agreement between MIPAS and MLS HNO_3 is within the range of −1.0 (−10%) to 1.0 ppbv (20%). MIPAS HNO_3 is 1.0 ppbv (10%) higher compared to MLS in the height range of 46 to 10 hPa over the Northern Hemisphere. Over the tropics at 31.6 hPa MLS shows a low bias of more than 1 ppbv (>50%). In general, MIPAS and MLS N_2O vmr agree within 20 to 40 ppbv (20 to 40%). Differences in the height range between 100

AMTD
2, 439–487, 2009

to 21 hPa are attributed to a known 20% positive bias in MIPAS N_2O data.

1 Introduction

Space-borne limb emission sounding is an established technique for monitoring the composition of the Earth's atmosphere above the middle troposphere. Its advantages are (1) high sensitivity to minor trace species, (2) good vertical resolution, (3) independence of sunlight, and, in consequence, the coverage of the whole earth within one day. Currently five limb emission instruments are orbiting the Earth: Sub-Millimeter Radiometer (SMR) on Odin (Murtagh et al., 2002), HIRDLS (High Resolution Dynamics Limb Sounder) (Gille et al., 2008), TES (Tropospheric Emission Spectrometer) (Beer et al., 2001), MLS (Microwave Limb Sounder) (Waters et al., 2006) on the EOS (Earth Observing System) Aura and MIPAS (Michelson Interferometer for Passive Atmospheric Sounding) (Fischer et al., 2008) on the Envisat satellite. SMR and MLS are operating in the sub-millimeter and microwave spectral region, while HIRDLS, TES, and MIPAS are mid-infrared instruments. Of those, TES has the capability of limb and nadir sounding and is mainly operated in nadir mode. HIRDLS, MLS, SMR and MIPAS are operating continuously. Most studies using limb-emission data have concentrated on the stratosphere and higher atmosphere, but recently the applicability to the region of the UTLS has been demonstrated by e.g. Glatthor et al. (2007); Jiang et al. (2007); von Clarmann et al. (2007); Eriksson et al. (2007); Su et al. (2006); Wu et al. (2005); Read et al. (2004, 1995).

Ceccherini et al. (2008) showed studies on the quality of MIPAS low resolution O_3 data and comparison with co-located measurements by GOMOS (Global Ozone Monitoring by Occultation of Stars). The present work shows comparisons of co-located measurements between the common retrieval quantities of MLS v2.2 and MIPAS low resolution data. This is a prerequisite for a possible combination of complementary parameters between the two instruments (e.g. differing trace gases, the same trace gases obstructed by thin clouds in case of mid-IR or by water vapour in case of microwave

observations). The emphasis is on the region of the upper troposphere to the middle stratosphere when MIPAS was operated in UTLS-1 mode.

2 MIPAS instrument and observations

MIPAS (Fischer et al., 2008) is a Fourier transform spectrometer taking high-spectral-resolution limb observations of the Earth's radiation from 685 cm^{-1} to 2410 cm^{-1} (14.6–4.15 μm). It was launched on 1 March 2002 on the Environmental satellite Envisat by the European Space Agency (ESA). It is orbiting in a sun-synchronous polar orbit at 800 km altitude with an inclination of 98.55° and an ascending equatorial crossing time of 10:00. From July 2002 until March 2004, MIPAS took measurements with maximum optical path difference (OPD) of 20 cm corresponding to a "high" spectral resolution of 0.025 cm^{-1}. During this time MIPAS measured mostly in its nominal mode, with a limb scan distance of ~500 km and 17 tangent heights covering an altitude range from 7 to 69 km. MIPAS provides nearly full global (or pole-to-pole) coverage with a latitude range of 87° S to 87° N. Due to problems with the interferometer mirror slide system, MIPAS performed few operations from April-December 2004. In January 2005 regular observations resumed, but with reduced duty cycle and a reduced spectral resolution (RR) of 0.0625 cm^{-1} (OPD=8.0 cm). The reduced spectral resolution has the advantage that more spectra can be measured during the same time interval compared to the former "high" spectral resolution observations. Various dedicated observation modes are being operated (http://www.atm.ox.ac.uk/group/mipas/rrmodes.html), most performing vertical oversampling intended for better sampling of the UTLS region.

In UTLS-1 mode MIPAS measures at 19 tangent points; tangent altitudes are latitude dependent from 7 to 50 km over the poles and 13 to 56 km over the equator. The vertical sampling grid spacing between the tangent altitudes is 1.5 km from 8.5 to 22 km, 2.0 km from 22 to 28 km, 3.0 km from 28 to 34 km and 4.5 km from 34 to 52 km. Thus, compared to the 3 km vertical field-of-view extent of MIPAS, an oversampling of up to a factor of 2 is achieved. As will be shown below, this leads to an improved vertical reso-

lution from 2 to 4 km in the UTLS region of the resulting trace gas profiles compared to the full resolution (FR) nominal mode observations.

2.1 MIPAS IMK-IAA data processing

Retrievals for temperature (T) and line-of-sight (LOS) in terms of the tangent point altitude, H_2O, O_3, HNO_3 and N_2O in the RR UTLS-1 mode were performed using the IMK/IAA data processor (von Clarmann et al., 2003) on the basis of ESA version IPF 4.67 calibrated radiance spectra. For the FR mode observations, the retrieval approach and comparisons/validation have been described in the following publications: T/LOS: von Clarmann et al. (2003), Wang et al. (2005); H_2O: Milz et al. (2005); O_3: Steck et al. (2007); HNO_3: Wang et al. (2007); N_2O: Glatthor et al. (2005). MIPAS retrievals make use of narrow wavelength regions (so-called microwindows) (Echle et al., 2000). The microwindows which were used for the evaluation of the FR measurements have been adapted to the RR UTLS-1 mode (Table 1). Further, cloud contaminated spectra are removed using the method of Spang et al. (2004).

The retrieval approach developed for the UTLS-1 mode parameters described here has been adopted as far as possible to the FR mode. Differences are related to the following items: (1) microwindows (Table 1), (2) zero-a-priori profiles for all the trace gases have been applied, (3) horizontal temperature inhomogeneities as gradient profiles derived from European Centre for Medium-Range Weather Forecasts (ECMWF) analysis are taken into account for all the trace gases, (4) as far as possible, altitude and latitude independent regularization (Steck and von Clarmann, 2001; Steck, 2000) is used and (5) in the case of H_2O, log(vmr) instead of vmr values are used as primary retrieval parameters. This helps in constraining the vmr profiles in spite of the large dynamic variation of H_2O in the upper troposphere.

2.1.1 Vertical resolution, horizontal resolution and error estimation

Figures 1 to 5 show the vertical resolution and the estimated measurement noise of temperature, H_2O, O_3, HNO_3 and N_2O distributions along one orbit in RR UTLS-1 mode (orbit 19595; 28–29 November 2005), compared with those of the FR nominal mode (orbit 09017; 21 November 2003). Up to ~30 km in the RR UTLS-1 mode, temperature and trace gas profiles have a vertical resolution of 2 to ~4 km due to vertical oversampling, degrading to ≥5 km further up due to the larger tangent point distance. In the case of FR nominal mode the vertical resolution is 3.5 to ~5 km up to ~40 km. The latitudinal wave-like pattern of the vertical resolution and estimated measurement noise in case of the RR UTLS-1 mode is caused by its latitude-dependent tangent altitude grid as described above. In comparison, such a structure does not appear in the figures for the FR nominal mode since there the tangent altitudes were fixed with latitude.

The estimated measurement noise is 0.2–0.3 K for temperature, 0.1–0.3 ppmv for H_2O, 0.03–0.09 ppmv for O_3, ~0.05 ppbv for HNO_3 and 4.0 ppbv for N_2O up to a height of 30 km in RR UTLS-1 mode. In the case of full resolution nominal mode the absolute noise error is generally higher than RR UTLS-1 mode (Figs. 1 to 5). The change in the vertical resolution and the estimated measurement noise with latitude (observed more prominently in the case of H_2O) is due to the MIPAS sensitivity to temperatures and the height constant regularization used. Because it is summer in the Southern Hemisphere during November-December, relatively better signal to noise ratio is observed compared to that in the Northern Hemisphere, accounting for latitudinal variation in the vertical resolution and estimated measurement noise.

Horizontal averaging kernels were derived in order to characterize the smoothing caused by the assumption of horizontal homogeneity in the limb observations (von Clarmann et al., 2009). We report (Table 2) the horizontal resolution of temperature and trace gases for a reference geolocation over the southern polar region (orbit 19306; 8 November 2005), in terms of full width at half maximum (FWHM) of the column of the

averaging kernel matrix (Rodgers, 2000; von Clarmann et al., 2009).

Tables 3 to 3 give results of the linear error analysis for temperature and trace gases calculated on the basis of a reference limb scan over mid-latitudes (7 November 2005; 01:35 UT). The total error is calculated as the quadratic sum of the mapping of the measurement noise onto the retrieval, errors due to interfering gases, temperature, temperature gradient, line-of-sight (LOS) uncertainties, spectral shift uncertainties, gain calibration uncertainties and error in the assumption about the instrument line shape (ILS). In the case of temperature the total error is dominated by the parameter error. In the case of H_2O, O_3, HNO_3 and N_2O parameter error is the main contributor to the total error up to 30 km, and LOS and temperature uncertainty are the dominant contributors to the parameter error in this height range. Above 30 up to 50 km measurement noise contributes significantly along with parameter error to the total error.

3 MLS instrument and data

Aura MLS was launched on 15 July 2004 into a near polar sun-synchronous orbit at altitude 705 km, with ascending equatorial crossing time of 13:45 (Schoeberl et al., 2006). It scans the Earth's limb providing 240 scans per orbit, spaced ~165 km along the orbit track, and ~3500 vertical profiles per day, with near pole-to-pole global latitudinal coverage from 82° S to 82° N. For this study we have used MLS version 2.2 (v2.2) data (Livesey et al., 2006). Most of the MLS data products are retrieved on a fixed vertical pressure grid with 6 levels per decade change in pressure from the troposphere to the stratosphere. In the case of temperature and H_2O, the vertical pressure grid is finer in the troposphere and the lower stratosphere, with 12 levels per decade change in pressure between 1000 to 22 hPa (0–25 km).

4 Comparisons

MIPAS RR UTLS-1 mode data and MLS v2.2 data for the period of November–December 2005 are used for comparisons. A coincidence criterion of ±12 h in time and ±300 km in space was used to find closely matched profiles between MIPAS and MLS. This gave to ∼300 to 350 coincident profiles over the poles/mid-latitudes and ∼50 to 250 matches over the sub-tropics and tropics. For MLS data, screening was done as specified in MLS v2.2 data quality document (http://mls.jpl.nasa.gov/data/datadocs.php). Since MIPAS and MLS have comparable vertical resolutions of ∼2 to 4 km in the region of the lower stratosphere, the profiles were compared directly without averaging kernel convolution (Rodgers, 2000).

To assess the validity of the comparison between the two instruments in the upper troposphere it is necessary to understand the influence of the a priori there. Since in case of MIPAS a Tikhonov-type (Tikhonov, 1963) formalism with a smoothing constraint is applied, a strong a-priori weighting would lead to a smoothing of the profile of the retrieved atmospheric parameter but not to any systematic bias. In case of MLS it has been tried to minimize the influence of the a-priori by relatively loose constraints. In case of MIPAS we can directly evaluate a priori influence in the troposphere by analysing each individual averaging kernel matrix. These are not available in case of MLS. However, in the MLS data product values are flagged where retrieved precision worse than 50% of the a priori precision indicates a large weight of the a priori information in the result. Such values were rejected from the comparison. For co-incident data points of MIPAS and MLS in the upper troposphere we have calculated the mean vertical resolution of MIPAS from the averaging kernel. This resulted in values of about 3 km for temperature, 2.5 km for H_2O, 2.2 km for O_3 and 2.6 km for HNO_3 in comparison to MLS values of 5 km (T), 1.5–3.5 km (H_2O), 3 km (O_3) and 3.5 km (HNO_3), as given in literature for altitudes below 100 hPa (Schwartz et al., 2008; Livesey et al., 2008; Read et al., 2007; Santee et al., 2007). N_2O is not considered here because quasi no significant amount of tropospheric co-incidences has been found. Thus, in the upper

troposphere, for the trace gases a direct comparison of the profiles from both instruments seems justified, while in case of temperature differences might be influenced by the differing vertical resolutions.

For the difference plots, first MIPAS altitude profiles of temperature and trace gases have been interpolated to the MLS pressure grid. Then for each pressure level the mean difference (MIPAS-MLS) of coincident profiles was calculated for each 5° latitude bin. These differences were plotted within the common pressure ranges of MLS and MIPAS as denoted by the black lines at the bottom and top in the difference plots. The percentage differences and the bias between MIPAS and MLS are calculated as suggested by von Clarmann (2006).

The bias is determined from the equation:

$$b_j = \frac{1}{N_j} \sum_{i=1}^{N_j} \left[x_{ij}^{\mathrm{MIPAS}} - x_{ij}^{\mathrm{MLS}} \right] \quad (1)$$

where b_j and N_j are the bias and total number of coincident geolocations at j-th pressure level of MLS. $x_{ij}^{\mathrm{MIPAS}} - x_{ij}^{\mathrm{MLS}}$ are the difference values obtained from MIPAS and MLS i-th coincident profile pairs, at the j-th pressure level of MLS.

Percentage differences are determined with respect to mean MLS values:

$$b_j^{\mathrm{perc}} = \frac{b_j N_j}{\sum_{i=1}^{N_j} x_{ij}^{\mathrm{MLS}}} \times 100. \quad (2)$$

The uncertainty of the bias is reported in terms of the standard error of the mean (SEM), assuming independent differences:

$$\mathrm{SEM}_j = \frac{\sigma_j}{\sqrt{N_j}} \quad (3)$$

where σ_j is the standard deviation of the bias:

$$\sigma_j = \sqrt{\frac{\sum_{i=1}^{N_j} \left[x_{ij}^{\mathrm{MIPAS}} - x_{ij}^{\mathrm{MLS}} - b_j\right]^2}{(N_j - 1)}}. \quad (4)$$

4.1 Temperature

MIPAS and MLS temperature fields from November to December 2005 and their difference are shown in Fig. 6. Vertical oscillations typically up to ±3 K are observed between MIPAS and MLS in the pressure/latitude range from 316.2 to 100.0 hPa and ~90° S to 90° N respectively. MIPAS is colder by up to 1 K than MLS at the 21.5 hPa pressure level. In the middle and upper stratosphere the agreement between MIPAS and MLS is between ±3 K. In aggregate, differences up to ±3 K in the UTLS and in the stratosphere are in agreement with the differences observed in MLS in comparison to other satellite instruments (Schwartz et al., 2008).

Figure 7 shows differences (MIPAS-ECMWF) and (MLS-ECMWF) interpolated on to the MLS pressure grid. The agreement of MIPAS with ECMWF is within ±1.5 K while MLS temperatures show vertical oscillations of ±3 K w.r.t ECMWF analysis below 10.0 hPa. Above 10.0 hPa poor agreement is seen between MIPAS and ECMWF with differences of −4 K up to ≤12 K. MLS also shows similar poor agreement w.r.t ECMWF especially over the poles. Since the latitude dependence and magnitude of these differences w.r.t ECMWF are similar in case of MLS and MIPAS, they are probably due to errors in the ECMWF analysis dataset.

The global mean altitude dependent bias between MIPAS and MLS temperatures is shown in Fig. 8. The overall mean biases are within ±2.5 K from the upper troposphere to the upper stratosphere. By comparison to the SEM (plotted as error bars but not visible as values are ≪1) all mean biases are significant.

4.2 H_2O

In Fig. 9 and Fig. 10 global 2-d distributions of MIPAS and MLS H_2O, and their zonal differences are shown. Between 316.2 to 177.8 hPa (Fig. 10) over the mid-latitudes and poles MIPAS is wetter compared to MLS by about 50% (up to 100%), more prominently over the Southern Hemisphere. From 215.4 to 177.8 hPa over the sub-tropics and tropics MIPAS H_2O vmr's are drier by ∼10% compared to MLS.

Our MIPAS/MLS comparison, in the lower stratosphere (146.7–56.2 hPa; Fig. 9) shows oscillations of ±1 ppmv (±10%), over all latitudes. This "band" of oscillating values is seen to vary in altitude at different latitudes. Oscillations up to 10% are observed between 31.6–26.1 hPa for all latitudes. In the middle and upper stratosphere between 26.1–0.2 hPa the agreement between MIPAS and MLS is within ±5%.

Read et al. (2007), have also observed AIRS to be consistently wetter in comparison to MLS over the high latitudes in the pressure range 316 to 178 hPa. The oscillations observed in the height range 31.6 to 26.1 hPa are due to a known artefact in MLS H_2O v2.2 retrievals (Lambert et al., 2007).

Figure 11 shows the global mean and relative bias between MIPAS and MLS H_2O. Overall, the derived mean biases within ±12% from the troposphere to the upper stratosphere and are significant.

4.3 Relative humidity over ice

Comparisons of tropical upper tropospheric relative humidity over ice (RHi) between MIPAS and MLS are shown in Fig. 12. MIPAS RHi profiles are computed using the formula by Goff and Gratch (1946) from MIPAS temperature and H_2O profiles. Over the tropics RHi up to 0.8–1 between 121.1 to 100.0 hPa are observed by MIPAS. In the case of MLS, RHi values of 0.8–1 are observed between 316.2 to 82.5 hPa and RHi >1 are observed from 68.1 up to 56.2 hPa. MIPAS/MLS (Fig. 12) differences of ±0.2 are observed between 146.7 to 68.1 hPa. For further investigations two sets of RHi profiles were computed: (1) using MIPAS temperature and MLS H_2O, and (2)

using MLS temperature and MIPAS H_2O. The difference MIPAS-set(1) showed a good agreement of 0 up to 0.1 (Fig. 13 (top)), while the difference MIPAS-set(2) (Fig. 13 (bottom)), showed similar large differences as the original comparison (Fig. 12). These Large differences between MLS and MIPAS mostly arise from the differences in the temperatures retrieved by the two instruments.

4.4 O_3

MIPAS and MLS O_3 zonal distributions and related differences are shown in Figs. 14 and 15. In the upper stratosphere (6.8–1.4 hPa) over the southern mid-latitudes and subtropics, MIPAS shows up to 10% higher values in comparison to MLS. Over the tropics at 31.6 hPa a difference (MIPAS-MLS) of 0.5 ppmv (~20%) is observed. Over the tropics and sub-tropics above the tropical tropopause layer (TTL) (100.0–68.1 hPa; Fig. 15) relative differences from ~90% to −80% are observed. Over the south pole in the height range 146.7 to 100.0 hPa differences up to 10% are observed.

A comparison of MLS O_3 profiles with MIPAS RR nominal mode observations has been published by Froidevaux et al. (2008). They observed differences up to 10% in the upper stratosphere which agrees with our analysis of the MIPAS RR UTLS-1 mode here. Froidevaux et al. (2008) also report differences up to ~5% (globally) between MLS and other instruments at the 21.5 hPa pressure level, which is also consistent with our comparison. However, we observe a positive difference of up to 20% at 31.6 hPa over the tropical region – a bias not appearing in the validation work by Froidevaux et al. (2008). The high relative differences over the tropics and sub-tropics in the TTL may partly be explained by low O_3 concentrations and strong vertical gradients in this region.

The global mean and relative bias of MIPAS/MLS O_3 and SEM are shown in Fig. 16. The overall bias including −18% up to <11% in the UT, are significant compared to the precision (SEM) of our comparison.

4.5 HNO_3

Mean global distributions and comparisons of MIPAS and MLS HNO_3 are presented in Fig. 17. In the UTLS region (146.7–68.1 hPa) agreement between MIPAS and MLS is within 0.5–1 ppbv; the high relative differences which are observed are due to the low absolute abundance. In the lower to the middle stratosphere (68.1–14.6 hPa) differences are typically within 1 ppbv and relative differences up to ∼10–20%, with an exception over the tropics. Over the tropics in the pressure range 31.6–21.5 hPa, differences of 1 ppbv (about 400%) are observed which could be due to very low values seen by MLS.

In the UTLS region the positive difference observed in MIPAS versus MLS is in agreement with the low bias present in MLS (Santee et al., 2007). It had been reported by Santee et al. (2007) that MLS is uniformly low by 10–30% in the stratosphere. The MIPAS/MLS deviations reported here are in agreement with other comparisons reported by Santee et al. (2007) with the exception of the tropics around 21.5 hPa. Kinnison et al. (2008) have also observed very similar high relative differences in comparison of MLS and HIRDLS over the tropics.

In the case of HNO_3, the global mean and relative bias of MIPAS/MLS and SEM are shown in Fig. 18. The overall mean bias is <20% in the middle stratosphere and is significant.

4.6 N_2O

The latitudinal distribution of N_2O vmr values of MIPAS and MLS and their related differences are shown in Fig. 19. In the lower stratosphere (100.0–21.5 hPa) MIPAS is typically up to 20% (≤60 ppbv) larger than MLS along all latitudes. From 21.5 to 10.0 hPa agreement between MIPAS and MLS is typically about 5% (20 ppbv) in most of the latitude bins, apart from the subtropics and the north pole, where relative differences up to −10% and 20% respectively, are observed. In the upper stratosphere (6.8–1.0 hPa) differences up to ±10 ppbv and high relative differences are observed.

The positive bias of ~10–15% in the lower stratosphere is attributed to the known positive bias in MIPAS retrievals (Payan et al., 2009; Glatthor et al., 2005). High relative differences observed in the upper stratosphere are due to low N_2O concentrations present in this region.

In the case of N_2O, the global mean and relative bias between MIPAS and MLS is <20% in the stratosphere and by comparison to the SEM all mean biases are significant, shown in Fig. 20.

5 Conclusions

IMK-IAA retrievals of temperature and trace gases from MIPAS reduced resolution (RR) UTLS-1 mode are shown. Vertical resolution and precisions of RR UTLS-1 mode are comparable to or better than MIPAS full resolution (FR) retrievals. The agreement between MIPAS and MLS is good with the exceptions of temperature at 121 hPa, relative humidity in the height range ~146 hPa to 68 hPa, O_3 in the tropical/sub-tropical lowermost stratosphere, HNO_3 over the tropics and N_2O in the height range 100 to 21 hPa.

Due to the similar altitude resolution and well characterized biases, the combination of MIPAS and MLS datasets seems possible. Since MIPAS trace gas observations at lower altitudes are in general more obstructed by clouds than those of MLS, synergistic use of MIPAS and MLS data can be useful e.g. in understanding H_2O/HNO_3 partitioning near tropical cirrus cloud and polar stratospheric cloud (PSC) studies. Further studies will indicate how far other species measured by both instruments provide a consistent picture of processes in the stratosphere and upper troposphere. If consistent, trace gases in the UTLS, such as CH_3CN which is observed by MLS, (although the reliability of the MLS v2.2 CH_3CN data has not yet been confirmed) and C_2H_2, C_2H_6, PAN which are observed by MIPAS will then be used to complement each other for global pollution monitoring studies.

Similarly, in the stratosphere, both instruments together have the power to cover a large set of major inorganic chlorine and bromine species consistently: the chlorine

species ClO (MLS, MIPAS), $ClONO_2$ (MIPAS) and HOCl (MIPAS, MLS), and HCl (MLS), or the bromine species BrO from MLS and, as discovered most recently, $BrONO_2$ from MIPAS (Höpfner et al., 2008), can be used to constrain halogen chemistry in models.

Acknowledgements. Re-processed MIPAS level-1B data were provided by ESA for scientific analysis. We gratefully acknowledge ECMWF for providing temperature field data and GES Distributed Active Archive Center for providing MLS temperature and trace gases data for comparison studies. This study has been funded by BMBF via contract no. 50 EE 0512 and by the EC project SCOUT-O3. The work at the Jet Propulsion Laboratory, California Institute of Technology was done under contract with NASA.

References

Beer, R., Glavich, T. A., and Rider, D. M.: Tropospheric emission spectrometer for the Earth Observing System's Aura satellite, Appl. Optics, 40, 2356–2367, 2001. 442

Ceccherini, S., Cortesi, U., Verronen, P. T., and Kyrölä, E.: Technical Note: Continuity of MIPAS-ENVISAT operational ozone data quality from full- to reduced-spectral-resolution operation mode, Atmos. Chem. Phys., 8, 2201–2212, 2008, http://www.atmos-chem-phys.net/8/2201/2008/. 442

Echle, G., von Clarmann, T., Dudhia, A., Flaud, J.-M., Funke, B., Glatthor, N., Kerridge, B., López-Puertas, M., Martín-Torres, F. J., and Stiller, G. P.: Optimized spectral microwindows for data analysis of the Michelson Interferometer for Passive Atmospheric Sounding on the Environmental Satellite, Appl. Optics, 39, 5531–5540, 2000. 444

Eriksson, P., Ekström, M., Rydberg, B., and Murtagh, D. P.: First Odin sub-mm retrievals in the tropical upper troposphere: ice cloud properties, Atmos. Chem. Phys., 7, 471–483, 2007, http://www.atmos-chem-phys.net/7/471/2007/. 442

Fischer, H., Birk, M., Blom, C., Carli, B., Carlotti, M., von Clarmann, T., Delbouille, L., Dudhia, A., Ehhalt, D., Endemann, M., Flaud, J. M., Gessner, R., Kleinert, A., Koopman, R., Langen, J., López-Puertas, M., Mosner, P., Nett, H., Oelhaf, H., Perron, G., Remedios, J., Ridolfi, M., Stiller, G., and Zander, R.: MIPAS: an instrument for atmospheric and climate research, Atmos. Chem. Phys., 8, 2151–2188, 2008, http://www.atmos-chem-phys.net/8/2151/2008/. 442, 443

Froidevaux, L., Jiang, Y., Lambert, A., Livesey, N., Read, W., Waters, J., Browell, E., Hair, J., Avery, M., McGee, T., Twigg, L., Sumnicht, G., Jucks, K., Margitan, J., Sen, B., Stachnik, R., Toon, G., Bernath, P., Boone, C., Walker, K., Filipiak, M., Harwood, R., Fuller, R., Manney, G., Schwartz, M., Daffer, W., Drouin, B., Cofield, R., Cuddy, D., Jarnot, R., Knosp, B., Perun, V., Snyder, W., Stek, P., Thurstans, R., and Wagner, P.: Validation of Aura Microwave Limb Sounder stratospheric ozone measurements, J. Geophys. Res., 113, D15S20, doi:10.1029/2007JD008771, 2008. 451

Gille, J., Barnett, J., Arter, P., Barker, M., Bernath, P., Boone, C., Cavanaugh, C., Chow, J., Coffey, M., Craft, J., Craig, C., Dials, M., Dean, V., Eden, T., Edwards, D., Francis, G., Halvorson, C., Harvey, L., Hepplewhite, C., Khosravi, R., Kinnison, D., Krinsky, C., Lambert, A., Lee, H., Lyjak, L., Loh, J., Mankin, W., Massie, S., McInerney, J., Moorhous, J., Nardi, B., Packman, D., Randall, C., Reburn, J., Rudolf, W., Schwartz, M., Serafin, J., Stone, K., Torpy, B., Walker, K., Waterfall, A., Watkins, R., Whitney, J., Woodard, D., and Young, G.: The High Resolution Dynamics Limb Sounder (HIRDLS): Experiment Overview, Recovery and Validation of Initial Temperature Data, J. Geophys. Res., 113, D16S43, doi:10.1029/2007JD008824, 2008. 442

Glatthor, N., von Clarmann, T., Fischer, H., Funke, B., Grabowski, U., Höpfner, M., Kellmann, S., Kiefer, M., Linden, A., Milz, M., Steck, T., Stiller, G. P., Mengistu Tsidu, G., and Wang, D. Y.: Mixing processes during the Antarctic vortex split in September/October 2002 as inferred from source gas and ozone distributions from ENVISAT-MIPAS, J. Atmos. Sci., 62, 787–800, 2005. 444, 453

Glatthor, N., von Clarmann, T., Fischer, H., Funke, B., Grabowski, U., Höpfner, M., Kellmann, S., Kiefer, M., Linden, A., Milz, M., Steck, T., and Stiller, G. P.: Global peroxyacetyl nitrate (PAN) retrieval in the upper troposphere from limb emission spectra of the Michelson Interferometer for Passive Atmospheric Sounding (MIPAS), Atmos. Chem. Phys., 7, 2775–2787, 2007, http://www.atmos-chem-phys.net/7/2775/2007/. 442

Goff, J. A. and Gratch, S.: Low-pressure properties of water from −160 to 212 F, in: Transactions of the American society of heating and ventilating engineers, presented at: 52nd Annual Meeting of the American Society of Heating and Ventilating Engineers New York, 95–122, 1946. 450

Höpfner, M., Orphal, J., von Clarmann, T., Stiller, G., and Fischer, H.: Stratospheric BrONO2 observed by MIPAS, Atmos. Chem. Phys. Discuss., 8, 19679–19705, 2008, http://www.atmos-chem-phys-discuss.net/8/19679/2008/. 454

Jiang, J. H., Livesey, N. J., Su, H., Neary, L., McConnell, J. C., and Richards, N. A. D.: Connecting surface emissions, conrective uplifting and long–range transport of carbon monoxide in the upper troposphere: New observations from the Aura Microwave Limb Sounder, Geophys. Res. Lett., 34, L18812, doi:10.1029/2007GL030638, 2007. 442

Kinnison, D., Gille, J., Barnett, J., Randall, C., Harvey, V., Lambert, A., Khosravi, R., Alexander, M., Bernath, P., Boone, C., Cavanaugh, C., Coffey, M., Craig, C., Dean, V., Eden, T., Ellis, D., Fahey, D., Francis, G., C. Halvorson, J. H., Hartsough, C., Hepplewhite, C., Krinsky, C., Lee, H., Mankin, W., Marcy, T., Massie, S., Nardi, B., Packman, D., Popp, P., Santee, M., Yudin, V., and Walker, K.: Global Observations of HNO3 from the High Resolution Dynamics Limb Sounder (HIRDLS) – First results, J. Geophys. Res., 113, D16S44, doi:10.1029/2007JD008814, 2008. 452

Lambert, A., Read, W., Livesey, N., Santee, M., Manney, G., Froidevaux, L., Wu, D., Schwartz, M., Pumphrey, H., Jimenez, C., Nedoluha, G., Cofield, R., Cuddy, D., Daffer, W., Drouin, B., Fuller, R., Jarnot, R., Knosp, B., Pickett, H., Perun, V., Snyder, W., Stek, P., Thurstans, R., Wagner, P., Waters, J., Jucks, K., Toon, G., Stachnik, R., Bernath, P., Boone, C., Walker, K., Urban, J., Murtagh, D., Elkins, J., and Atlas, E.: Validation of the Aura Microwave Limb Sounder middle atmosphere water vapor and nitrous oxide measurements, J. Geophys. Res., 112, D24S36, doi:10.1029/2007JD008724, 2007. 450

Livesey, N., Snyder, W., Read, W., and Wagner, P.: Retrieval algorithms for the EOS Microwave Limb Sounder (MLS) instrument, IEEE Trans. Geosci. Remote Sensing, 44, 1144–1155, 2006. 446

Livesey, N. J., Filipiak, M. J., Froidevaux, L., Read, W. G., Lambert, A., Santee, M. L., Jiang, J. H., Pumphrey, H. C., Waters, J. W., Cofield, R. E., Cuddy, D. T., Daffer, W. H., Drouin, B. J., Fuller, R. A., Jarnot, R. F., Jiang, Y. B., Knosp, B. W., Li, Q. B., Perun, V. S., Schwartz, M. J., Snyder, W. V., Stek, P. C., Thurstans, R. P., Wagner, P. A., Avery, M., Browell, E. V., Cammas, J.-P., Christensen, L. E., Diskin, G. S., Gao, R.-S., Jost, H.-J., Loewenstein, M., Lopez, J. D., Nedelec, P., Osterman, G. B., Sachse, G. W., and Webster, C. R.: Validation of Aura Microwave Limb Sounder O_3 and CO observations in the upper troposphere and lower stratosphere, J. Geophys. Res., 113, D15S02, doi:10.1029/2007JD008805, 2008. 447

Milz, M., von Clarmann, T., Fischer, H., Glatthor, N., Grabowski, U., Höpfner, M., Kellmann, S., Kiefer, M., Linden, A., Mengistu Tsidu, G., Steck, T., Stiller, G. P., Funke, B., López-Puertas, M., and Koukouli, M. E.: Water Vapor Distributions Measured with the Michelson Interferometer for Passive Atmospheric Sounding on board Envisat (MIPAS/Envisat), J. Geophys. Res.,

110, D24307, doi:10.1029/2005JD005973, 2005. 444
Murtagh, D., Frisk, U., Merino, F., Ridal, M., Jonsson, A., Stegman, J., Witt, G., Eriksson, P., Jiménez, C., Megie, G., de la Nöe, J., Ricaud, P., Baron, P., Pardo, J. R., Hauchcorne, A., Llewellyn, E. J., Degenstein, D. A., Gattinger, R. L., Lloyd, N. D., Evans, W. F. J., McDade, I. C., Haley, C. S., Sioris, C., von Savigny, C., Solheim, B. H., McConnell, J. C., Strong, K., Richardson, E. H., Leppelmeier, G. W., Kyrölä, E., Auvinen, H., and Oikarinen, L.: An overview of the Odin atmospheric mission, Can. J. Phys., 80, 309–319, doi:10.1139/P01-157, 2002. 442
Payan, S., Camy-Peyret, C., Oelhaf, H., Wetzel, G., Maucher, G., Keim, C., Pirre, M., Huret, N., Engel, A., Volk, M. C., Kuellmann, H., Kuttippurath, J., Cortesi, U., Bianchini, G., Mencaraglia, F., Raspollini, P., Redaelli, G., Vigouroux, C., De Mazière, M., Mikuteit, S., Blumenstock, T., Velazco, V., Notholt, J., Mahieu, E., Duchatelet, P., Smale, D., Wood, S., Jones, N., Piccolo, C., Payne, V., Bracher, A., Glatthor, N., Stiller, G., Grunow, K., Jeseck, P., Te, Y., and Butz, A.: Validation of version-4.61 methane and nitrous oxide observed by MIPAS, Atmos. Chem. Phys., 9, 413–442, 2009, http://www.atmos-chem-phys.net/9/413/2009/. 453
Read, W., Lambert, A., Bacmeister, J., Cofield, R., Christensen, L., Cuddy, D., Daffer, W., Drouin, B., Fetzer, E., Froidevaux, L., Fuller, R., Herman, R., Jarnot, R., Jiang, J., Jiang, Y., Kelly, K., Knosp, B., Pumphrey, H., Rosenlof, K., Sabounchi, X., Santee, M., Schwartz, M., Snyder, W., Stek, P., Su, H., Takacs, L., Thurstans, R., Vomel, H., Wagner, P., Waters, J., Webster, C., Weinstock, E., and Wu, D.: Aura Microwave Limb Sounder upper tropospheric and lower stratospheric H2O and relative humidity with respect on ice validation, J. Geophys. Res. 112, D24S35, doi:10.1029/2007JD008752, 2007. 447, 450
Read, W. G., Waters, J. W., Froidevaux, L., Flower, D. A., Jarnot, R. F., Hartmann, D. L., Harwood, R. S., and Rood, R. B.: Upper-tropospheric water vapor from UARS MLS, B. Am. Meteorol. Soc., 76, 2381–2389, 1995. 442
Read, W. G., Wu, D. L., Waters, J. W., and Pumphrey, H. C.: Dehydration in the tropical tropopause layer: Implications from the UARS Microwave Limb Sounder, J. Geophys. Res., 109, D06110, doi:10.1029/2003JD004056, 2004. 442
Rodgers, C. D.: Inverse Methods for Atmospheric Sounding: Theory and Practice, in: Series on Atmospheric, Oceanic and Planetary Physics, Vol. 2, edited by: Taylor, F. W., World Scientific, 2000. 446, 447
Santee, M., Lambert, A., Read, W., Livesey, N., Cofield, R., Cuddy, D., Daffer, W., Drouin, B.,

Froidevaux, L., Fuller, R., Jarnot, R., Knosp, B., Manney, G., Perun, V., Snyder, W., Stek, P., Thurstans, R., Wagner, P., Waters, J., Muscari, G., deZafra, R., Dibb, J., Fahey, D., Popp, P., Marcy, T., Jucks, K., Toon, G., Stachnik, R., Bernath, P., Boone, C., Walker, K., Urban, J., and Murtagh, D.: Validation of Aura Microwave Limb Sounder HNO3 Measurements, J. Geophys. Res., 112, D24S40, doi:10.1029/2007JD008721, 2007. 447, 452

Schoeberl, M., Douglass, A., Hilsenrath, E., Bhartia, P., Barnett, J., Beer, R., Waters, J., Gunson, M., Froidevaux, L., Gille, J., Levelt, P., and DeCola, P.: Overview of the EOS Aura Mission, IEEE Trans. Geosci. Remote Sensing, 44, 1066–1074, 2006. 446

Schwartz, M., Lambert, A., Manney, G., Read, W., Livesey, N., Froidevaux, L., Ao, C., Bernath, P., Boone, C., Cofield, R., Daffer, W., Drouin, B., Fetzer, E., Fuller, R., Jarnot, R., Jiang, J., Jiang, Y., Knosp, B., Kruger, K., Li, J.-L., Mlynczak, M., Pawson, S., III, J. R., Santee, M., Snyder, W., Stek, P., Thurstans, R., Tompkins, A., Wagner, P., Walker, K., Waters, J., and Wu, D.: Validation of the Aura Microwave Limb Sounder Temperature and Geopotential Height Measurements, J. Geophys. Res., 113, D15S11, doi:10.1029/2007JD008783, 2008. 447, 449

Spang, R., Remedios, J. J., and Barkley, M. P.: Colour indices for the detection and differentiation of cloud types in infra–red limb emission spectra, Adv. Space Res., 3, 1041–1047, doi:10.1016/S0273-1177(03)00585-4, 2004. 444

Steck, T.: Bestimmung von Vertikalprofilen von Spurengasen aus MIPAS–Messungen unter Hinzunahme von a priori Wissen, Ph.D. thesis, Institut für Meteorologie und Klimaforschung, Universität Karlsruhe, Kernforschungszentrum Karlsruhe, dissertation, DLR-FB 2000–01, ISSN 1434-8454, 2000. 444

Steck, T. and von Clarmann, T.: Constrained profile retrieval applied to the observation mode of the Michelson Interferometer for Passive Atmospheric Sounding, Appl. Optics, 40, 3559–3571, 2001. 444

Steck, T., von Clarmann, T., Fischer, H., Funke, B., Glatthor, N., Grabowski, U., Höpfner, M., Kellmann, S., Kiefer, M., Linden, A., Milz, M., Stiller, G. P., Wang, D. Y., Allaart, M., Blumenstock, Th., von der Gathen, P., Hansen, G., Hase, F., Hochschild, G., Kopp, G., Kyrö, E., Oelhaf, H., Raffalski, U., Redondas Marrero, A., Remsberg, E., Russell III, J., Stebel, K., Steinbrecht, W., Wetzel, G., Yela, M., and Zhang, G.: Bias determination and precision validation of ozone profiles from MIPAS-Envisat retrieved with the IMK-IAA processor, Atmos. Chem. Phys., 7, 3639–3662, 2007, http://www.atmos-chem-phys.net/7/3639/2007/. 444

Su, H., Read, W. G., Jiang, J. H., Waters, J. W., Wu, D. L., and Fetzer, E. J.: Enhanced positive water vapor feedback associated with tropical deep convection: New evidence from Aura MLS, Geophys. Res. Lett., 33, L05709, doi:10.1029/2005GL025505, 2006. 442

Tikhonov, A.: On the solution of incorrectly stated problems and method of regularization, Dokl. Akad. Nauk. SSSR, 151, 501–504, 1963. 447

von Clarmann, T.: Validation of remotely sensed profiles of atmospheric state variables: strategies and terminology, Atmos. Chem. Phys., 6, 4311–4320, 2006, http://www.atmos-chem-phys.net/6/4311/2006/. 448

von Clarmann, T., Glatthor, N., Grabowski, U., Höpfner, M., Kellmann, S., Kiefer, M., Linden, A., Mengistu Tsidu, G., Milz, M., Steck, T., Stiller, G. P., Wang, D. Y., Fischer, H., Funke, B., Gil-López, S., and López-Puertas, M.: Retrieval of temperature and tangent altitude pointing from limb emission spectra recorded from space by the Michelson Interferometer for Passive Atmospheric Sounding (MIPAS), J. Geophys. Res., 108, 4736, doi:10.1029/2003JD003602, 2003. 444

von Clarmann, T., Glatthor, N., Koukouli, M. E., Stiller, G. P., Funke, B., Grabowski, U., Höpfner, M., Kellmann, S., Linden, A., Milz, M., Steck, T., and Fischer, H.: MIPAS measurements of upper tropospheric C_2H_6 and O_3 during the southern hemispheric biomass burning season in 2003, Atmos. Chem. Phys., 7, 5861–5872, 2007, http://www.atmos-chem-phys.net/7/5861/2007/. 442

von Clarmann, T., De Clercq, C., Ridolfi, M., Höpfner, M., and Lambert, J.-C.: The horizontal resolution of MIPAS, Atmos. Meas. Tech., 2, 47-54, 2009. 445, 446

Wang, D. Y., von Clarmann, T., Fischer, H., Funke, B., Gil-López, S., Glatthor, N., Grabowski, U., Höpfner, M., Kaufmann, M., Kellmann, S., Kiefer, M., Koukouli, M. E., Linden, A., López-Puertas, M., Mengistu Tsidu, G., Milz, M., Steck, T., Stiller, G. P., Simmons, A. J., Dethof, A., Swinbank, R., Marquardt, C., Jiang, J. H., Romans, L. J., Wickert, J., Schmidt, T., Russell III, J., and Remsberg, E.: Validation of stratospheric temperatures measured by Michelson Interferometer for Passive Atmospheric Sounding MIPAS on Envisat, J. Geophys. Res., 110, D08301, doi:10.1029/2004JD005342, 2005. 444

Wang, D. Y., Höpfner, M., Mengistu Tsidu, G., Stiller, G. P., von Clarmann, T., Fischer, H., Blumenstock, T., Glatthor, N., Grabowski, U., Hase, F., Kellmann, S., Linden, A., Milz, M., Oelhaf, H., Schneider, M., Steck, T., Wetzel, G., López-Puertas, M., Funke, B., Koukouli, M. E., Nakajima, H., Sugita, T., Irie, H., Urban, J., Murtagh, D., Santee, M. L., Toon, G., Gunson, M. R., Irion, F. W., Boone, C. D., Walker, K., and Bernath, P. F.: Validation of

nitric acid retrieved by the IMK-IAA processor from MIPAS/ENVISAT measurements, Atmos. Chem. Phys., 7, 721–738, 2007, http://www.atmos-chem-phys.net/7/721/2007/. 444

Waters, J., Froidevaux, L., Harwood, R., Jarnot, R., Pickett, H., Read, W., Siegel, P., Cofield, R., Filipiak, M., Flower, D., Holden, J., Lau, G., Livesey, N., Manney, G., Pumphrey, H., Santee, M., Wu, D., Cuddy, D., Lay, R., Loo, M., Perun, V., Schwartz, M., Stek, P., Thurstans, R., Boyles, M., Chandra, S., Chavez, M., Chen, G.-S., Chudasama, B., Dodge, R., Fuller, R., Girard, M., Jiang, J., Jiang, Y., Knosp, B., LaBelle, R., Lee, K., Miller, D., Oswald, J., Patel, N., Pukala, D., Quintero, O., Scaff, D., Snyder, W., Tope, M., Wagner, P., and Walch, M.: The Earth Observing System Microwave Limb Sounder (EOS MLS) on the Aura satellite, IEEE Trans. Geosci. Remote Sens., 44, 2006. 442

Wu, D., Read, W., Dessler, A., Sherwood, S., and Jiang, J.: UARS MLS Cloud Ice Measurements and Implications for H2O Transport near the Tropopause, J. Atmos. Sci., 62, 518–530, 2005. 442

Table 1. Microwindows selected for MIPAS low resolution data for UTLS 1 mode.

Gases	MIPAS Bands used	Microwindows in the range (cm^{-1})
temperature	A (685–970)	(731.25–812.56)
H_2O	A (685–970), B (1215–1500), C (1570–1750)	(795.75–1603.43)
O_3	A (685–970), AB (1020–1170)	(760.69–1039.00)
HNO_3	A (685–970)	(862.50–812.56)
N_2O	B (1215–1500)	(1227–1304)

Table 2. Horizontal resolution in terms of full width at half maximum of the column of the horizontal averaging kernels.

Single scan of orbit 19306 on 8 November 2005 over the southern polar latitudes.

Altitude (km)	T (km)	H_2O (km)	O_3 (km)	HNO_3 (km)	N_2O (km)
10	173	146	317	209	97
15	113	210	155	280	241
20	197	122	347	321	226
30	102	117	365	150	107
40	170	111	200	119	183
50	111	76	431	77	83

Table 3a. Error budget determined for a single scan of orbit 19281 on 7 November 2005 in the northern mid-latitudes for selected altitudes.

Temperature			
Altitude (km)	Total error[a]	Measurement noise	Parameter error[b]
10	3.4	0.32	3.4
15	1.2	0.27	1.1
20	0.59	0.28	0.52
30	0.59	0.31	0.51
40	0.92	0.45	0.81
50	1.5	0.88	1.2

[a] Total errors are the quadratic combination of measurement noise and parameter error and are given in K.
[b] Parameter error is the quadratic combination of error contributions from interfering gases which are not jointly fitted, and from spectral shift, gain calibration and instrumental line-shape uncertainties.

Table 3b.

H_2O					
Altitude (km)	Total error[a]	Measurement noise	Parameter error[b]	Line-of-sight (LOS)[c]	Temp.[d]
10	5.1 (32)	0.57 (4)	5 (31)	4.8 (31)	1.1 (7)
15	0.35 (7)	0.16 (3)	0.32 (7)	0.28 (6)	0.08 (2)
20	0.26 (6)	0.15 (3)	0.21 (5)	0.19 (4)	0.05 (1)
30	0.43 (8)	0.31 (6)	0.3(6)	0.19 (3)	0.16 (3)
40	0.75 (11)	0.67 (9)	0.34 (5)	0.06 (1)	0.02 (<1)
50	0.86 (23)	0.57 (15)	0.64 (15)	0.03 (3)	0.2 (3)

[a] Total errors are the quadratic combination of measurement noise and parameter error. Absolute values of the total error are in ppmv and relative values are given in parentheses (%).

[b] Parameter error is the quadratic combination of error contributions from interfering gases which are not jointly fitted, and from temperature, temperature gradient, LOS (in terms of tangent point altitude), spectral shift, gain calibration and instrumental line-shape uncertainties.

[c] Based on tangent altitude uncertainty of 150 m. LOS uncertainties contribute to the parameter errors but are given explicitly because of their dominant role.

[d] Based on temperature uncertainty of 1 K. Temperature uncertainties contribute to the parameter errors but are given explicitly because of their dominant role.

Table 3c.

O_3					
Altitude (km)	Total error[a]	Measurement noise	Parameter error[b]	Line-of-sight (LOS)[c]	Temp.[d]
10	0.04 (114)	0.04 (105)	0.02 (41)	0 (26)	0 (15)
15	0.05 (7)	0.03 (5)	0.04 (6)	0.04 (5)	0.01 (1.5)
20	0.10 (4)	0.04 (2)	0.09 (3)	0.04 (1)	0.01 (<1)
30	0.35 (5)	0.09 (1)	0.34 (5)	0.25 (4)	0.11 (2)
40	0.43 (7)	0.07 (1)	0.43 (7)	0.22 (4)	0.25 (4)
50	0.23 (5)	0.05 (4)	0.22 (3)	0.11 (2)	0.07 (<1)

[a] Total errors are the quadratic combination of measurement noise and parameter error. Absolute values of the total error are in ppmv and relative values are given in parentheses (%).

[b] Parameter error is the quadratic combination of error contributions from interfering gases which are not jointly fitted, and from temperature, temperature gradient, LOS (in terms of tangent point altitude), spectral shift, gain calibration and instrumental line-shape uncertainties.

[c] Based on tangent altitude uncertainty of 150 m. LOS uncertainties contribute to the parameter errors but are given explicitly because of their dominant role.

[d] Based on temperature uncertainty of 1 K. Temperature uncertainties contribute to the parameter errors but are given explicitly because of their dominant role.

Table 3d.

HNO_3					
Altitude (km)	Total error[a]	Measurement noise	Parameter error[b]	Line-of-sight (LOS)[c]	Temp.[d]
10	0.06 (11)	0.04 (7)	0.05 (8)	0.05 (8)	0.01 (2)
15	0.12 (5)	0.05 (2)	0.11 (4)	0.09 (3)	0.01 (<1)
20	0.24 (3)	0.06 (<1)	0.24 (3)	0.11 (1)	0.05 (<1)
30	0.37 (5)	0.09 (1)	0.36 (5)	0.33 (5)	0.09 (1)
40	0.16 (27)	0.14 (24)	0.06 (10)	0.05 (8)	0 (<1)
50	0.29 (163)	0.26 (153)	0.12 (63)	0.03 (20)	0.04 (20)

[a] Total errors are the quadratic combination of measurement noise and parameter error. Absolute values of the total error are in ppmv and relative values are given in parentheses (%).

[b] Parameter error is the quadratic combination of error contributions from interfering gases which are not jointly fitted, and from temperature, temperature gradient, LOS (in terms of tangent point altitude), spectral shift, gain calibration and instrumental line-shape uncertainties.

[c] Based on tangent altitude uncertainty of 150 m. LOS uncertainties contribute to the parameter errors but are given explicitly because of their dominant role.

[d] Based on temperature uncertainty of 1 K. Temperature uncertainties contribute to the parameter errors but are given explicitly because of their dominant role.

Table 3e.

N_2O					
Altitude (km)	Total error[a]	Measurement noise	Parameter error[b]	Line-of-sight (LOS)[c]	Temp.[d]
10	20 (6)	8.9 (3)	18 (5)	17 (5)	0.25 (<1)
15	17 (5)	6.1 (2)	15 (5)	10 (3)	9.7 (3)
20	15 (9)	4.8 (2)	14 (8)	13 (7)	4.8 (4)
30	7.5 (9)	3.1 (3)	6.9 (8)	5.3 (6)	3.5 (4)
40	2.6 (13)	1.6 (8)	2.1 (10)	0.5 (3)	0.2 (2)
50	1 (83)	0.6 (52)	0.8 (61)	0.05 (7)	0.2 (18)

[a] Total errors are the quadratic combination of measurement noise and parameter error. Absolute values of the total error are in ppmv and relative values are given in parentheses (%).

[b] Parameter error is the quadratic combination of error contributions from interfering gases which are not jointly fitted, and from temperature, temperature gradient, LOS (in terms of tangent point altitude), spectral shift, gain calibration and instrumental line-shape uncertainties.

[c] Based on tangent altitude uncertainty of 150 m. LOS uncertainties contribute to the parameter errors but are given explicitly because of their dominant role.

[d] Based on temperature uncertainty of 1 K. Temperature uncertainties contribute to the parameter errors but are given explicitly because of their dominant role.

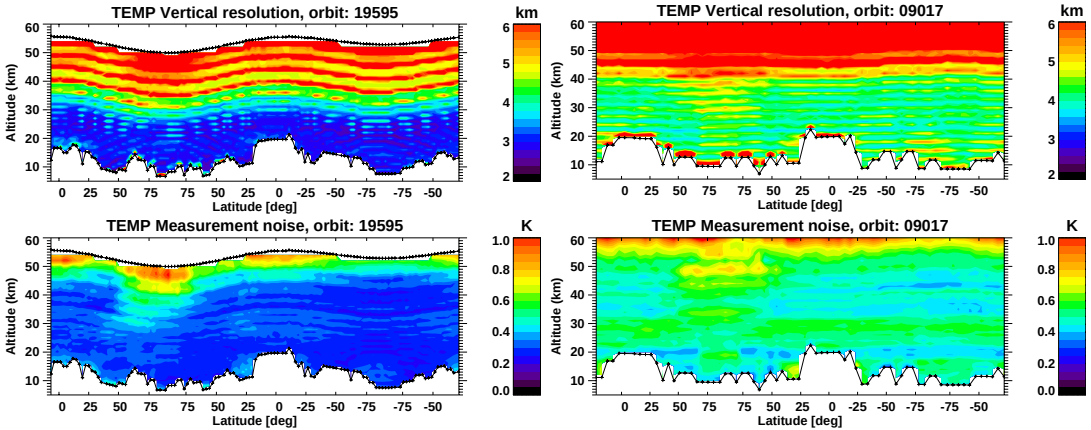

Fig. 1. Vertical resolution of temperature on 28–29 November 2005 obtained from one single orbit 19595 in MIPAS RR mode (upper left) and for 21 November 2003 from orbit 09017 in FR mode (upper right). Corresponding retrieved measurement noise in RR mode (lower left) and FR mode (lower right).

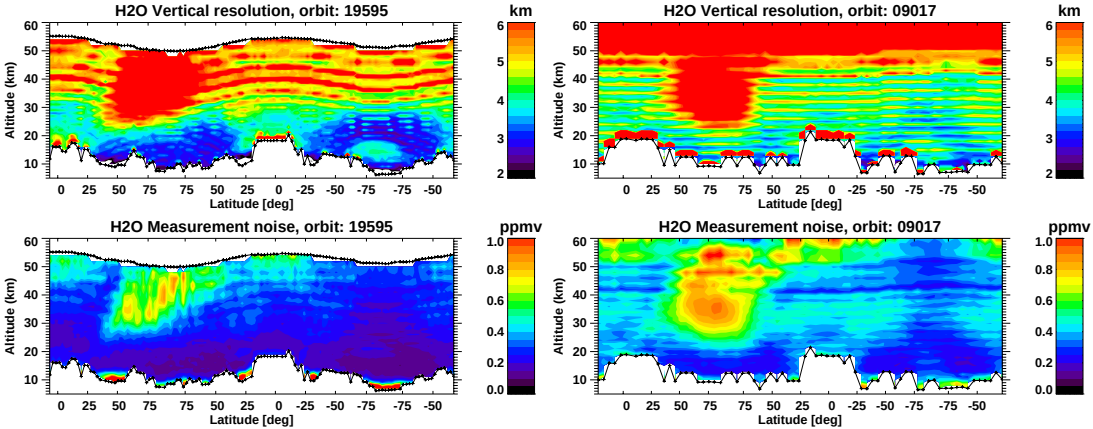

Fig. 2. Vertical resolution of H_2O on 28–29 November 2005 obtained from one single orbit 19595 in MIPAS RR mode (upper left) and for 21 November 2003 from orbit 09017 in FR mode (upper right). Corresponding retrieved measurement noise in RR mode (lower left) and FR mode (lower right).

AMTD
2, 439–487, 2009

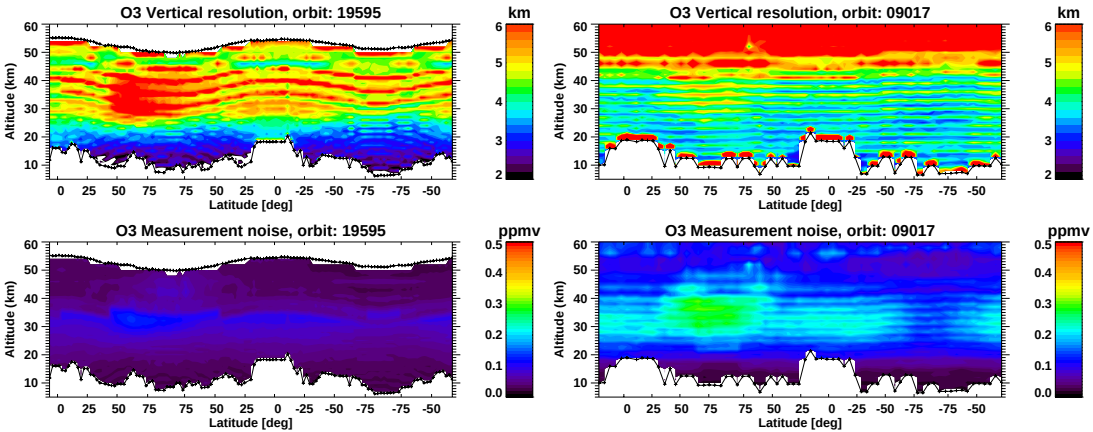

Fig. 3. Vertical resolution of O_3 on 28–29 November 2005 obtained from one single orbit 19595 in MIPAS RR mode (upper left) and for 21 November 2003 from orbit 09017 in FR mode (upper right). Corresponding retrieved measurement noise in RR mode (lower left) and FR mode (lower right).

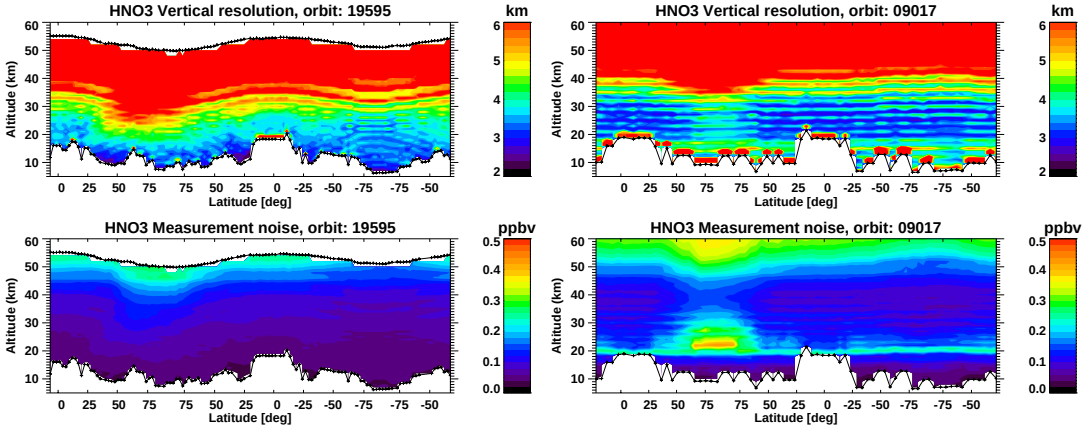

Fig. 4. Vertical resolution of HNO_3 on 28–29 November 2005 obtained from one single orbit 19595 in MIPAS RR mode (upper left) and for 21 November 2003 from orbit 09017 in FR mode (upper right). Corresponding retrieved measurement noise in RR mode (lower left) and FR mode (lower right).

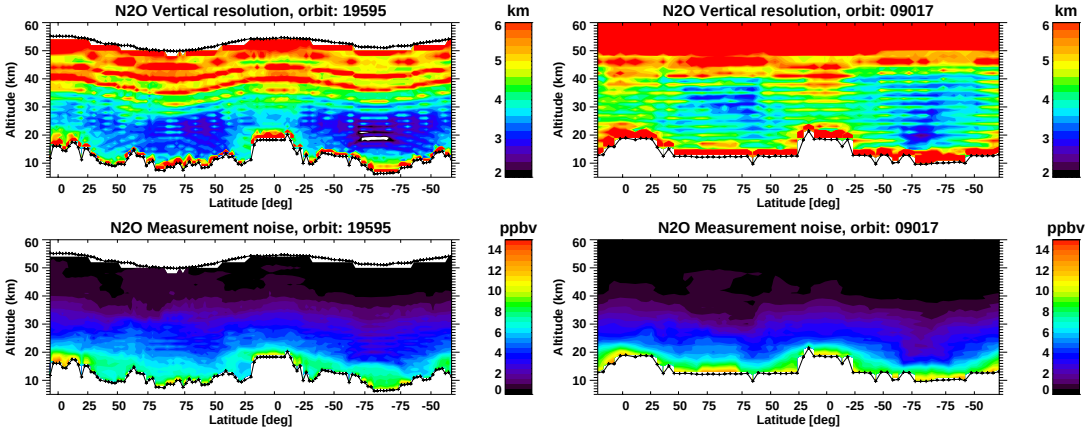

Fig. 5. Vertical resolution of N_2O on 28–29 November 2005 obtained from one single orbit 19595 in MIPAS RR mode (upper left) and for 21 November 2003 from orbit 09017 in FR mode (upper right). Corresponding retrieved measurement noise in RR mode (lower left) and FR mode (lower right).

AMTD
2, 439–487, 2009

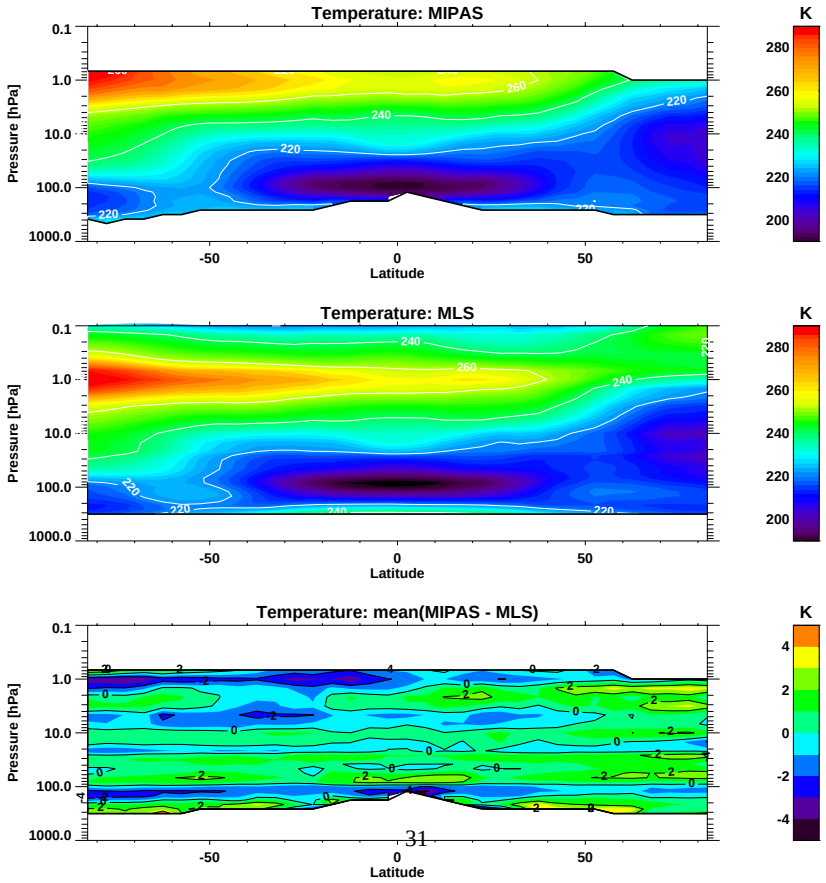

Fig. 6. Global temperature field from MIPAS (top) and MLS (middle) from 6 November to 7 December 2005 and their mean differences (bottom).

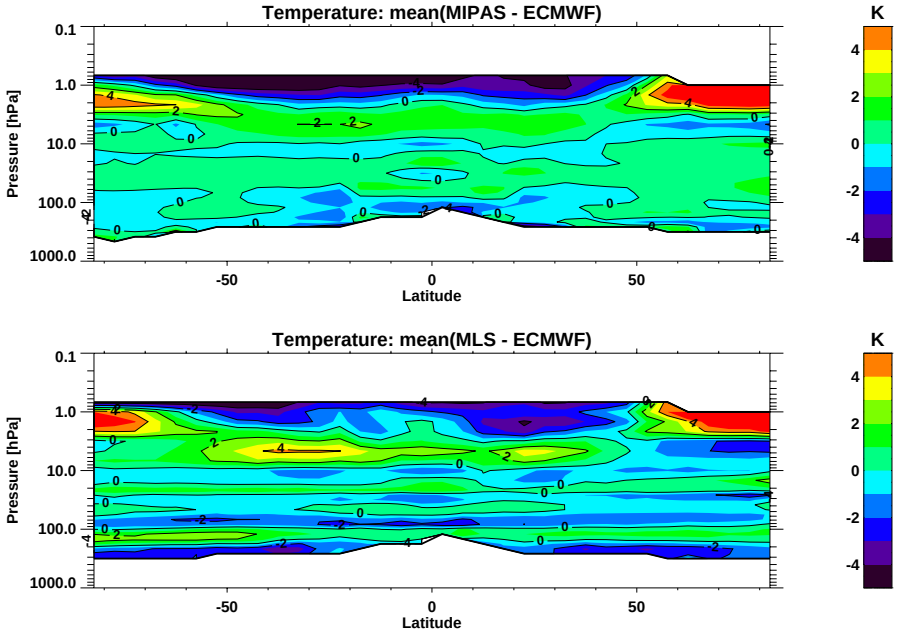

Fig. 7. Global mean differences for MIPAS-ECMWF temperatures (top) and MLS-ECMWF temperatures (bottom) from 6 November to 7 December 2005. Dark red and black colours represent values greater than +5 K and smaller than −4 K respectively.

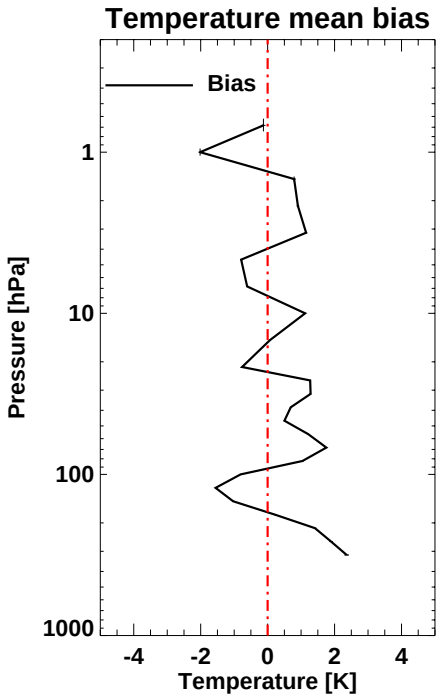

Fig. 8. Global mean bias (MIPAS-MLS) for temperatures for 6 November to 7 December 2005. The uncertainty of the bias (SEM) is plotted as error bars which are, however, too small to be resolved.

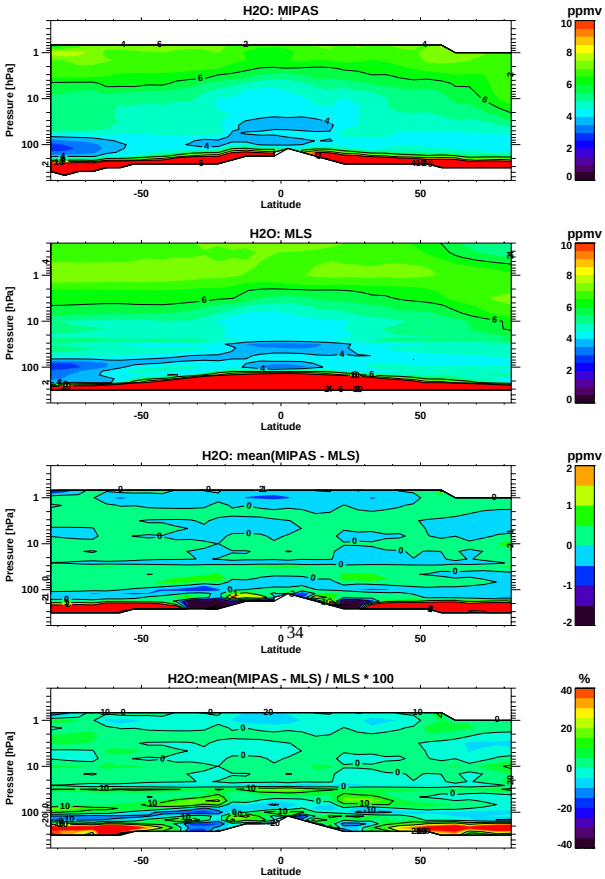

Fig. 9. Global H_2O field from MIPAS and MLS from 6 November to 7 December 2005. Mean differences and their relative differences. Colours beyond the colour scale (dark red and black) represent values outside the range of colour legend.

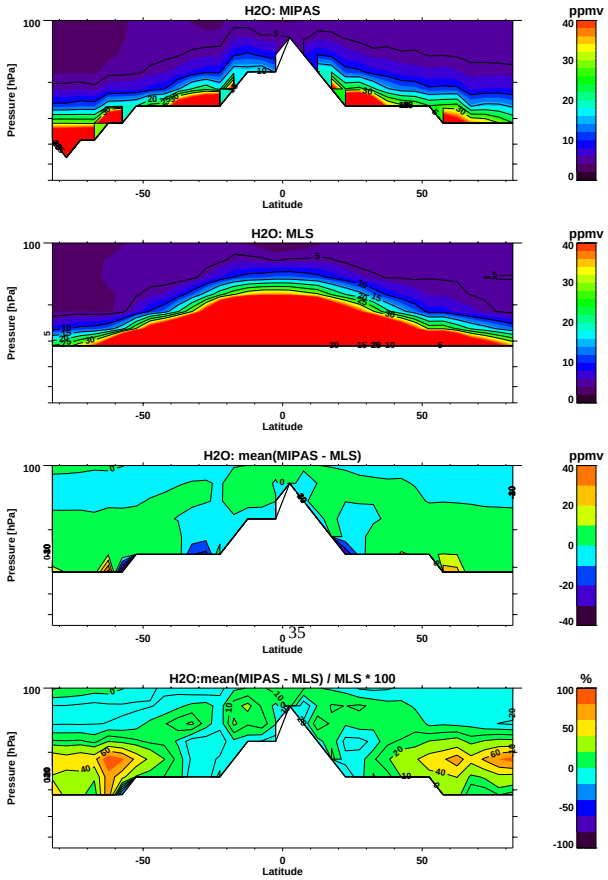

Fig. 10. Same as Fig. 8 but for UT.

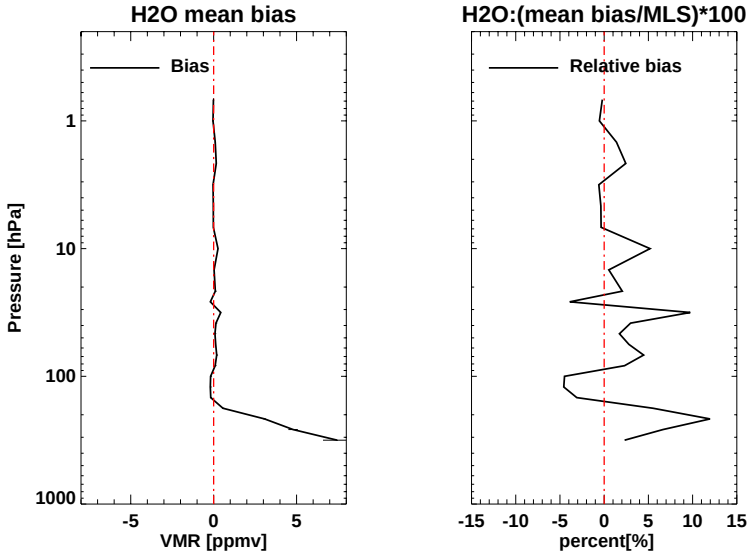

Fig. 11. Global mean bias (MIPAS-MLS) and relative bias for H_2O for 6 November to 7 December 2005. The uncertainty of the bias (SEM) is plotted as error bars which are, however, too small to show.

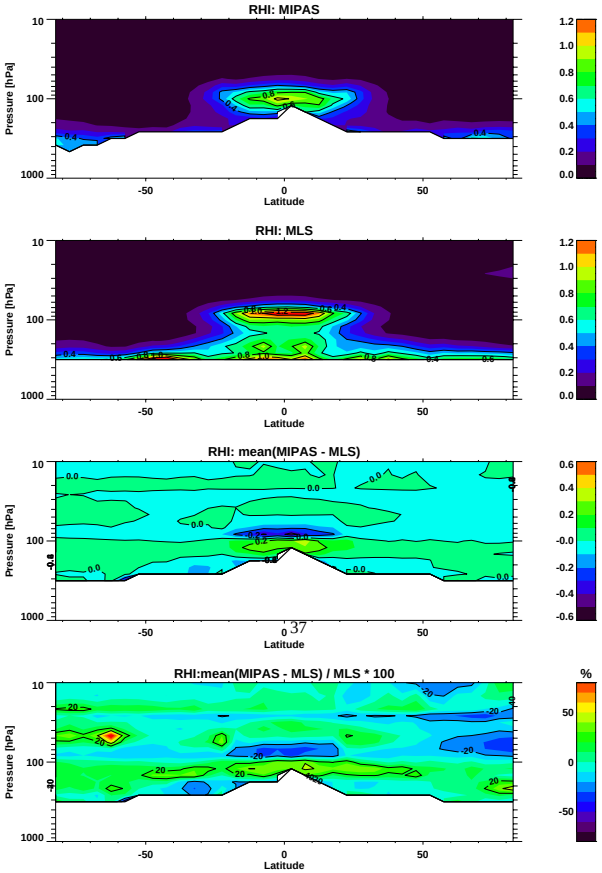

Fig. 12. Global RHi field from MIPAS and MLS from 6 November to 7 December 2005. Mean differences between MIPAS and MLS and their relative differences.

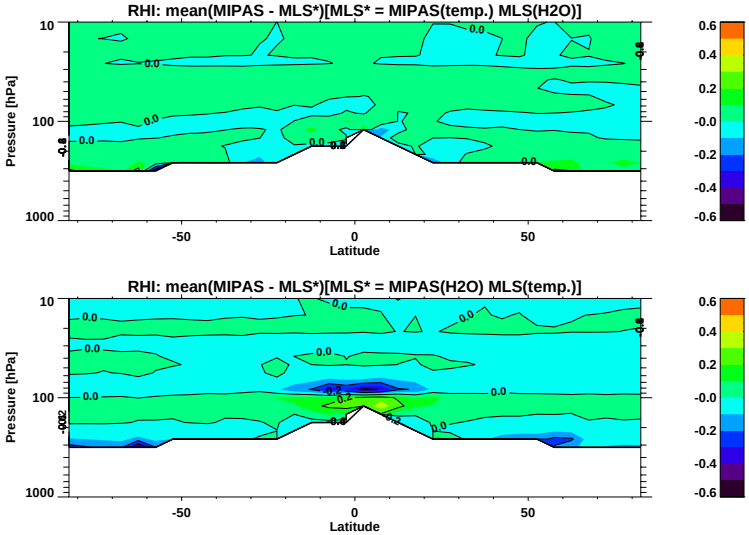

Fig. 13. Mean differences of MIPAS and MLS* RHI's (MIPAS-MLS*). In the top panel, RHI is computed using MIPAS temperature and MLS H_2O profiles. Incase of bottom plot, RHI is computed using MIPAS H_2O and MLS temperature profiles.

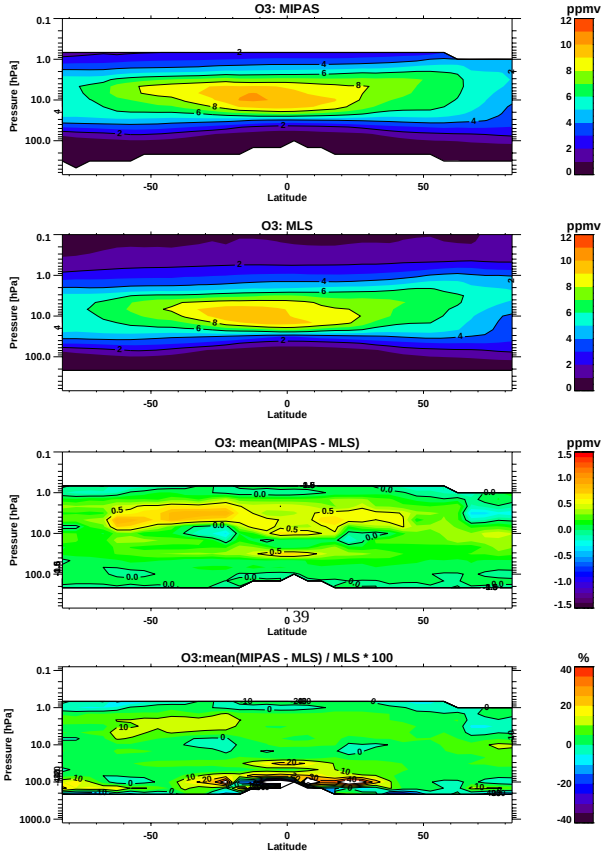

Fig. 14. Global O_3 field from MIPAS and MLS from 6 November to 7 December 2005. Mean differences between MIPAS and MLS and their relative differences. The white patches at 100 hPa correspond to values beyond the colour scale.

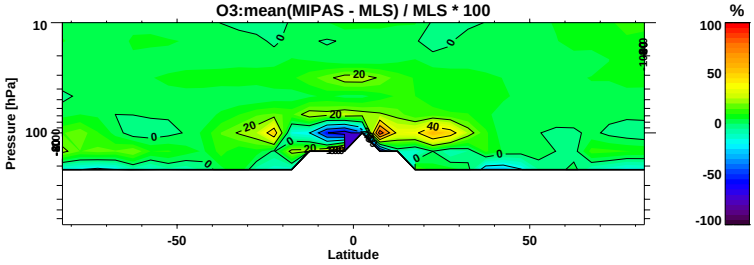

Fig. 15. Relative differences between MIPAS and MLS O_3 from 215 hPa–10 hPa.

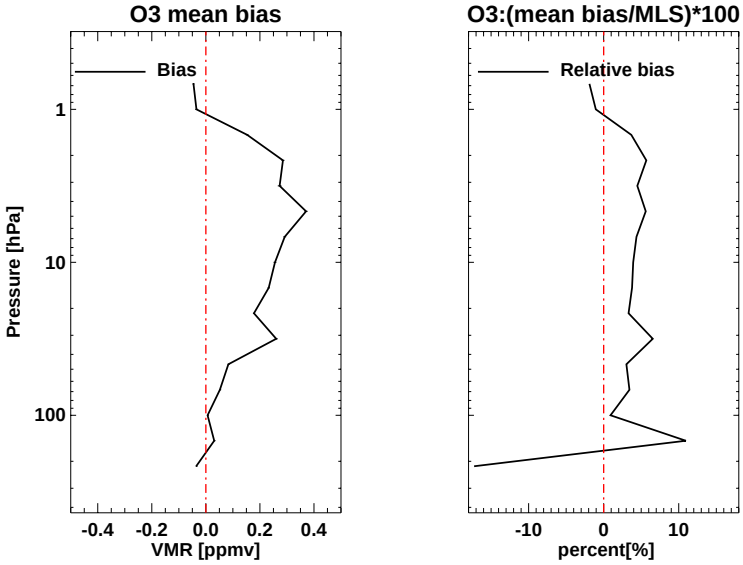

Fig. 16. Same as Fig. 11 but for O_3.

AMTD
2, 439–487, 2009

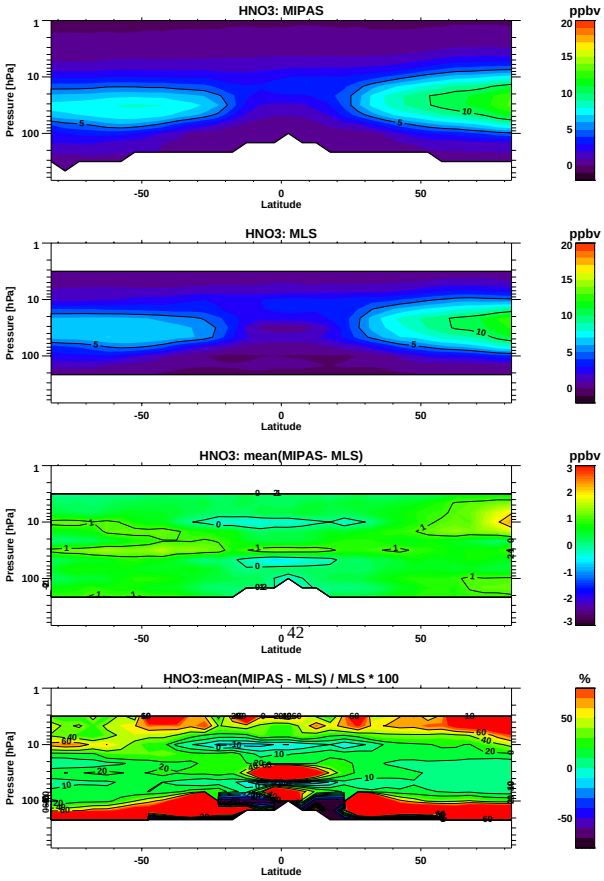

Fig. 17. Global HNO_3 field from MIPAS and MLS from 6 November to 7 December 2005. Mean differences between MIPAS and MLS and their relative differences. Colours beyond the colour scale (dark red and black) represent values outside the range of colour legend.

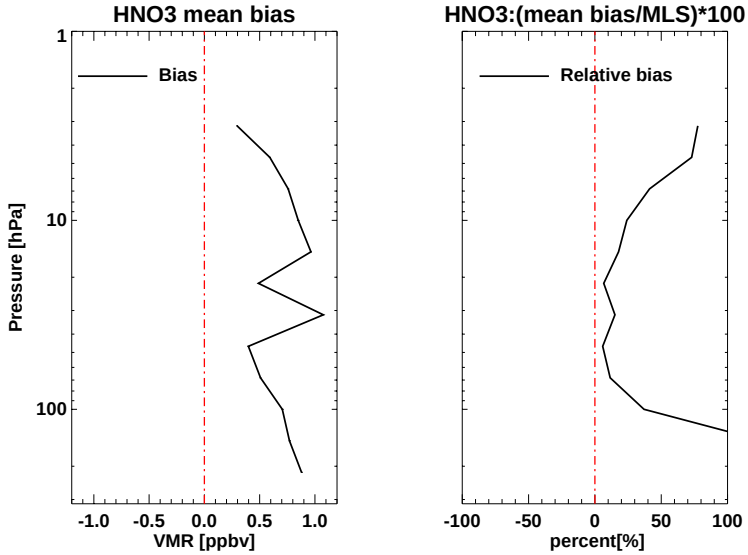

Fig. 18. Same as Fig. 11 but for HNO_3.

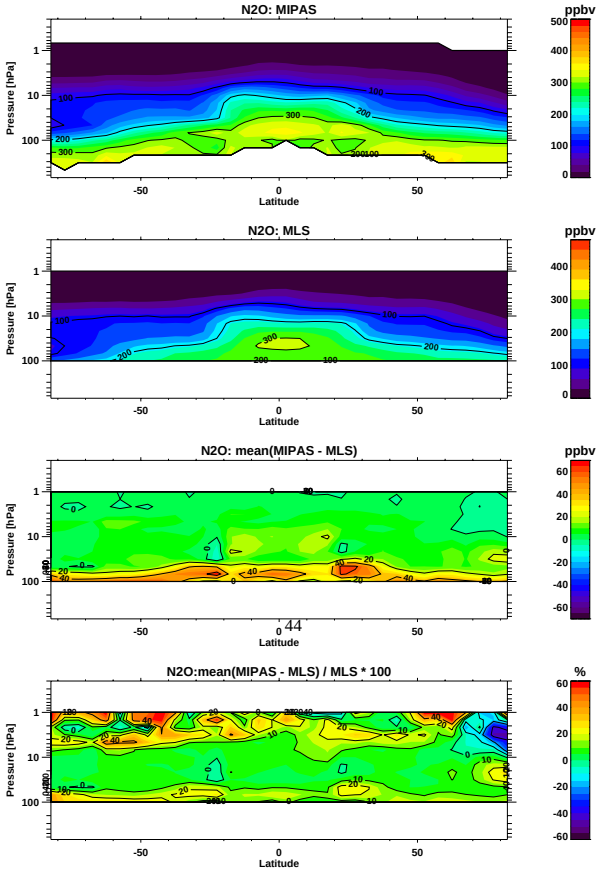

Fig. 19. Global N_2O field from MIPAS and MLS from 6 November to 7 December 2005. Mean differences between MIPAS and MLS and their relative differences. Colours beyond the colour scale (dark red and black) represent values outside the range of colour legend.

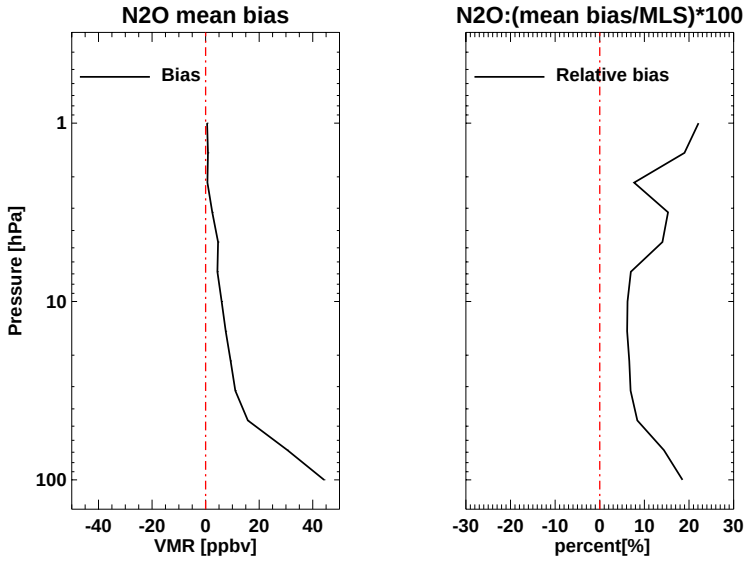

Fig. 20. Same as Fig. 11 but for N_2O.